



# High-strength and self-recoverable silk fibroin cryogels with anisotropic swelling and mechanical properties

Berkant Yetiskin, Oguz Okay \*

Department of Chemistry, Istanbul Technical University, 34469 Maslak, Istanbul, Turkey

## ARTICLE INFO

### Article history:

Received 1 June 2018

Received in revised form 1 September 2018

Accepted 14 September 2018

Available online 15 September 2018

### Keywords:

Anisotropy

Silk fibroin

Porous scaffolds

## ABSTRACT

Creating mechanically strong macroporous hydrogels with anisotropic properties as observed in many biological tissues is a major challenge in the gel science. Here we describe a directional freezing/cryogelation method of producing high-strength and rapid self-recoverable silk fibroin scaffolds with a high degree of mechanical anisotropy similar to that of tendon. By adjusting the synthesis parameters, we were able to create fibroin scaffolds exhibiting the highest modulus anisotropy so far reported,  $21 \pm 5$ , with moduli  $E = 2.3 \pm 0.5$  and  $0.11 \pm 0.03$  MPa measured along parallel and perpendicular to the freezing direction, respectively. The cryogels are squeezable under load whereas, upon unloading, the squeezed-out water is taken back immediately. It was shown that the squeezability of the cryogels results in significant viscous stresses and energy dissipation. Cyclic mechanical tests reveal that the friction between the fibroin pore walls is the primary factor responsible for the energy dissipation. Independent on the fibroin concentration or direction of the measurements, 60% of the mechanical energy given to the cryogels are dissipated due to the friction between the pore walls, which is responsible for their almost complete squeezability and self-recoverability.

© 2018 Elsevier B.V. All rights reserved.

## 1. Introduction

Hydrogels as soft and smart materials have important functions in a variety of biological and biomedical applications [1]. Significant progress has been made in the past decade in the development of mechanically strong and tough hydrogels with mechanical performances approaching those of biological systems [2]. The next important challenge to be addressed in the gel science is to create anisotropic microstructures and mechanical properties in high-strength hydrogels as observed in many tissues such as skin, muscle, and articular cartilage [3]. To evaluate the degree of mechanical anisotropy in natural and synthetic materials, one may measure a mechanical parameter such as the Young's modulus  $E$  in the directions parallel ( $\parallel$ ) and perpendicular ( $\perp$ ) to the orientation direction of the materials, and the ratio  $E_{\parallel}/E_{\perp}$  is referred to as the "modulus anisotropy" [3]. For instance, tendon, the connective tissue joining muscle to bone has a compressive  $E_{\parallel}/E_{\perp}$  ratio of around 20 [4], whereas human annulus fibrosus of intervertebral disk exhibits tensile circumferential moduli of 17.4 and 5.6 MPa at outer and inner sites, respectively, corresponding to  $E_{\parallel}/E_{\perp} = 3.1$  [5].

To create hydrogels with anisotropic microstructure and mechanical properties, several techniques have been developed such as stress-induced orientation, directional freezing, and self-assembly [3,6–20]. Hydrogels containing oriented clay nanotubes or fibrils exhibit modulus

anisotropy  $E_{\parallel}/E_{\perp}$  of 3.0 and 7.0, respectively [7,8]. Modulus anisotropies between 2 and 4 were also reported in polyvinyl alcohol and double-network hydrogels [9,10]. To our knowledge, the highest modulus anisotropy reported so far is 10.4, which was observed in polyacrylic acid hydrogels prepared by directional ice-crystal growing and subsequent polymerization [11]. These hydrogels are however mechanically weak, i.e., their moduli  $E_{\parallel}$  and  $E_{\perp}$  are 80.5 and 7.7 kPa, respectively. The utilization of anisotropic scaffolds as a biomaterial in tissue engineering applications should exhibit a modulus in the order of MPa to protect their integrity.

Silk fibroin is a promising and popular biomaterial due to its impressive biocompatibility, tunable biodegradability, outstanding thermomechanical stability, ease of processability, and remarkable mechanical properties [21–24]. Preparation of fibroin scaffolds with anisotropic mechanical properties is important in tissue engineering and bioseparation [25,26]. Anisotropic fibroin scaffolds were fabricated by directional freezing of aqueous fibroin solutions followed by freeze-drying to fix the oriented microstructure [27–29]. To render the scaffolds water-insoluble, they were then treated with methanol to induce the  $\beta$ -sheet formation. Although such scaffolds exhibit a high modulus anisotropy (up to 14), their Young's moduli are below kPa level, i.e.,  $E_{\parallel} = 0.28$  kPa, and  $E_{\perp} = 0.02$  kPa [27].

We recently reported an alternative strategy to create anisotropic fibroin scaffolds by combining directional freezing and cryogelation of aqueous fibroin solutions [30]. Cryogelation is a simple technique that provides formation of macroporous gels below the freezing point of

\* Corresponding author.  
E-mail address: [okayo@itu.edu.tr](mailto:okayo@itu.edu.tr) (O. Okay).

the gelation solution [31,32]. We have to mention that cryogelation and freezing/thawing are different techniques with respect to the formation mechanism and mechanical properties of polymeric scaffolds [31,32]. During cryogelation, the reactions occur in the unfrozen domains of the apparently frozen system occupying about 5% of the whole volume. Thus, the reactants such as fibroin are cryo-concentrated in these unfrozen domains where the gelation reactions proceed. The pore wall produced by cryogelation is a dense polymeric gel because of the cryoconcentrated fibroin solution around the ice crystals. In contrast, the pore wall formed after freezing/thawing of a conventional gel is a loosely crosslinked gel due to the absence of cryoconcentration. As a consequence, the porous structures produced during cryogelation are much stronger than those formed during freezing/thawing. For instance, Young's moduli of fibroin scaffolds formed via cryogelation and freezing/thawing of 4.2 wt% fibroin solutions are  $8 \pm 1$  and  $1.0 \pm 0.3$  MPa, respectively, highlighting the effect of cryoconcentration on the scaffold properties [34]. Moreover, cryogels can be squeezed almost completely without any crack propagation making them one of the toughest materials so far reported. We recently fabricated anisotropic silk fibroin scaffolds by immersing the reactor containing fibroin solution into a cold bath at a controlled rate followed by the cryogelation reactions [30]. By adjusting the immersion rate of the reactor into the cold bath, we were able to create anisotropic silk fibroin scaffolds with Young's moduli  $E$  in the range of MPa. However, their modulus anisotropy was below 4.3 due to the heat transfer to the reactor walls both in axial and radial directions [30].

Herein we report the preparation of silk fibroin scaffolds with a high degree of mechanical anisotropy similar to that of tendon together with a high mechanical strength and rapid self-recoverability. To prepare such hydrogels we designed a reactor consisting of a copper bottom plate and a cylindrical polytetrafluoroethylene (PTFE) mold exhibiting a thermal conductivity ratio of 1600 (Fig. 1a). Copper bottom plate was immersed in a cold bath at  $-30$  or  $-196$  °C, whereas the cylindrical PTFE mold locating outside of the cold bath was filled with aqueous solutions of silk fibroin of various concentrations together with butanediol diglycidyl ether (BDDE) and  $N,N,N',N'$ -tetramethylethylenediamine (TEMED) as a crosslinker and pH regulator, respectively [33–35]. Unidirectional frozen fibroin solution was then subjected to cryogelation at  $-18$  °C to induce a conformational transition in fibroin from random

coil to  $\beta$ -sheet structures and hence water stability [33]. As will be seen below, we were able to create mechanically strong silk fibroin scaffolds exhibiting microstructural, swelling and mechanical anisotropies. The scaffolds exhibit the highest modulus anisotropy so far reported,  $21 \pm 5$ , with moduli  $E = 2.3 \pm 0.5$  and  $0.11 \pm 0.03$  MPa measured along parallel and perpendicular to the freezing direction, respectively. We also demonstrate that, independent on the fibroin concentration or direction of the measurements, 60% of the mechanical energy given to the cryogels are dissipated due to the friction between the fibroin pore walls, which is responsible for their squeezability and self-recoverability.

## 2. Experimental

### 2.1. Materials

Butanediol diglycidyl ether (BDDE, Sigma-Aldrich),  $N,N,N',N'$ -tetramethylethylenediamine (TEMED, Sigma-Aldrich), LiBr (Merck), and  $\text{Na}_2\text{CO}_3$  (Merck) were used without further purification. Silk fibroin (SF) was isolated from *Bombyx mori* cocoons (Kozabirlik, Turkey) as described before [36]. Briefly, cocoons were first boiled in aqueous solution of 0.02 M  $\text{Na}_2\text{CO}_3$  for 1 h to remove sericin followed by rinsing the remaining SF with water at 70 °C. After dissolving SF in aqueous solution of 9.3 M LiBr at 60 °C for 2 h, the solution was dialyzed using a 100,000 MWCO dialysis tubing (Snake Skin, Pierce) for 3 days against water that was changed three times a day. After centrifugation, the final SF concentration was  $\sim 5$  wt%, which was determined by weighing the remaining solid after drying. Aqueous solutions with a higher SF concentration were prepared by concentrating 5 wt% SF solution via dialysis against aqueous solutions of 10 and 15 w/v% poly (ethylene glycol) (PEG, Sigma-Aldrich, molecular weight:  $\sim 10,000$  g mol $^{-1}$ ) using 3500 MWCO dialysis tubing (Snake Skin, Pierce). All SF solutions were stored at 4 °C and used within 2 weeks.

### 2.2. Preparation of anisotropic fibroin cryogels

Fibroin cryogels were prepared from aqueous solutions of fibroin at various concentrations  $C_{\text{SF}}$  in the presence of BDDE (20 mmol epoxide groups per gram of fibroin) and TEMED (0.25 v/v%). At  $C_{\text{SF}} = 16.7$  wt%,

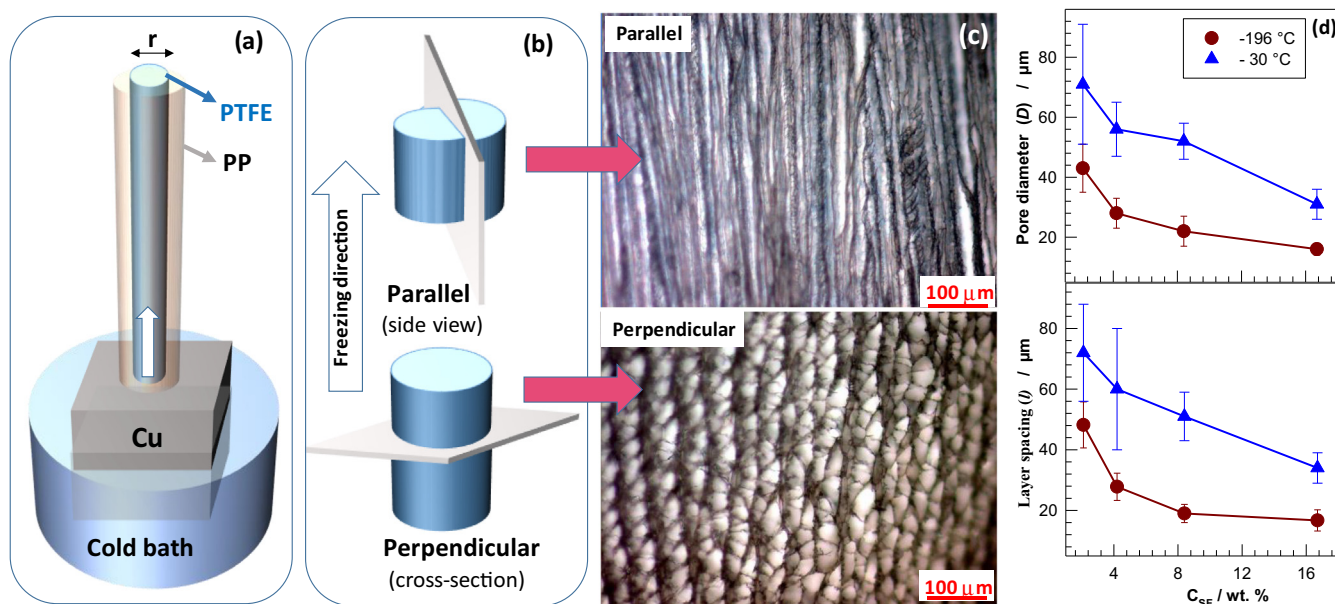


Fig. 1. (a): Experimental setup for the preparation of anisotropic fibroin cryogels. (b): Directions parallel and perpendicular to the freezing direction indicated by the white arrow. (c) Optical microscopy images of fibroin cryogels taken parallel and perpendicular to the freezing direction.  $C_0 = 4.2$  wt%. (d) Average pore diameter  $D$  and layer spacing  $l$  for cryogels prepared by freezing at  $-196$  °C (circles) and  $-30$  °C (triangles) plotted against the fibroin concentration  $C_{\text{SF}}$ .

BDDE concentration was decreased to 10 mmol g<sup>-1</sup> to prevent early gelation. As detailed before [33,34], BDDE acts as a cross linker to induce conformational transition in fibroin while TEMED is a pH regulator accelerating this transition. We have to note that gelation of aqueous fibroin solutions was studied before at various pH's between 6 and 11, which was adjusted by the addition of TEMED as a pH regulator [33]. The reactions between the amino groups on silk fibroin and the diepoxide crosslinker was found to be very fast and the resulting gels were mechanically strong in the presence of 0.25 v/v% TEMED producing a pH in the reaction solution of 10.2. We fixed this pH value together with the type of the pH-regulator throughout this study."

Typically, to obtain cryogels at C<sub>SF</sub> = 4.2 wt%, BDDE (0.50 mL) and TEMED (15 μL) were added to 5 mL of 5 wt% SF solution followed by adjusting the final volume to 6 mL with water. The homogeneous solution was then pipetted into a cylindrical polytetrafluoroethylene (PTFE) mold of 12 mm in internal diameter fitted with a copper bottom plate, as schematically shown in Fig. 1a. Preliminary experiments showed that the diameter of PTFE mold is also critical because thinner molds resulted in the formation of randomly distributed pores (Fig. S1). To further reduce the heat transfer in radial direction, a polypropylene (PP) pipe was placed around the PTFE mold and the copper part of the system was then immersed in a cold bath until the reaction system completely freezes which required around 30–45 min. Liquid nitrogen (−196 °C) and ethylene glycol/water mixture at equal volume ratio (−30 °C) were used as the cold bath in our experiments. Because the thermal conductivity of copper is 1600 fold larger than that of PTFE, freezing of the solution occurs in bottom-up direction. The reactor was then removed from the cold bath and placed in a cryostat at −18 °C to carry out the cryogelation reactions for 1 day. The gel specimens after preparation were thawed at 24 °C for 30 min and then immersed in excess of water for one week by refreshing water several times to extract any soluble species. The equilibrium swollen gel samples were taken out of water and freeze-dried to constant weight.

### 2.3. Characterization of fibroin cryogels

Swelling and gel fraction measurements as well as the conformational analysis of fibroin in the cryogels were carried out as reported before [35] (for details, see Supporting Information). Differential scanning calorimetry (DSC) measurements were conducted on a Perkin Elmer Diamond DSC under a nitrogen atmosphere. The cryogel samples equilibrium swollen in water were cut into specimens of about 10 mg wet weight and sealed in aluminum pans. They were then scanned between −50 and 250 °C with heating/cooling rates of 5 and 10 °C min<sup>-1</sup>. Thermal gravimetric analysis was conducted on a Labsys evo SETARAM system under nitrogen by heating from 20 to 500 °C at a rate of 10° min<sup>-1</sup>. Rheological measurements were conducted on a Bohlin Gemini 150 rheometer system (Malvern Instruments, UK) equipped with a Peltier device for temperature control. The gel specimens equilibrium swollen in water were placed between the parallel plates (diameter, 20 mm) of the instrument. During all of the rheological tests, a solvent trap was used and the outside of the upper plate was covered with a thin layer of low-viscosity silicone oil to prevent evaporation of water. To investigate the microstructural anisotropy, cylindrical cryogel specimens after freeze-drying were cut in directions parallel and perpendicular to the freezing direction, as schematically illustrated in Fig. 1b. The cut surfaces were then investigated using scanning electron microscopy (SEM) at various magnifications in a field emission scanning electron microscope (JEOL JSM-6510LV) after coating with gold for 3 min using a Sputter coater. The cut surfaces were also studied using an image analyzing system consisting of a microscope (XSZ single Zoom microscope), a CDD digital camera (TK 1381EG) and a PC with the data analyzing system Image-Pro Plus.

For the uniaxial compression tests, the cryogel specimens were cut into rectangular shapes (3.1 ± 0.4 × 2.9 ± 0.3 × 2.8 ± 0.4 mm) and compressed parallel and perpendicular to the freezing direction at a

constant crosshead speed  $\dot{\epsilon}$  of 0.3 mm min<sup>-1</sup>. The tests were performed at 24 ± 2 °C on a Zwick Roell test machine using a 500 N load cell. Before the test, an initial compressive contact to 0.01 ± 0.002 N was applied to ensure a complete contact between the gel and the plates. Compressive stress was presented by its nominal  $\sigma_{nom}$  and true values  $\sigma_{true}$  ( $=\lambda\sigma_{nom}$ ) which are the forces per cross-sectional area of the undeformed and deformed gel specimen, respectively, and  $\lambda$  is the deformation ratio (deformed length/original length). The compressive strain  $\epsilon$  is defined as the change in the length of the gel specimen relative to its initial length, i.e.,  $\epsilon = 1 - \lambda$ . The Young's modulus  $E$  was calculated from the slope of stress-strain curves between 2 and 4% compressions. The fracture nominal stress  $\sigma_f$  and fracture strain  $\epsilon_f$  were calculated from the maxima in  $\sigma_{true} - \epsilon$  plots, as detailed previously [30]. Cyclic mechanical tests were carried out with a compression step performed at a constant crosshead speed of 0.3 mm min<sup>-1</sup> to maximum strain  $\epsilon_{max}$  (varied between 20 and 80%), followed by immediate retraction to zero displacement and a waiting time of 5 min, until the next cycle of compression. Note that uniaxial tensile tests could not be conducted on the cryogel specimens because they were too slippery.

## 3. Results and discussion

### 3.1. Microstructure of fibroin cryogels

The experimental setup shown schematically in Fig. 1a provided formation of highly anisotropic silk fibroin (SF) cryogels. This could be achieved by use of the copper bottom plate of high conductivity preventing ice growth in the radial direction. Unidirectional freezing of the reaction system in liquid nitrogen (−196 °C) or ethylene glycol/water mixture (−30 °C) followed by cryogelation at −18 °C resulted in SF cryogels containing pore channels aligned to the freezing direction. Fig. 1c shows typical optical images of cryogel specimens prepared at a fibroin concentration C<sub>SF</sub> of 4.2 wt% using liquid nitrogen as the cold bath. The images were taken parallel and perpendicular to the freezing direction corresponding to the vertical section along the aligned fibroin channels and the cross-section of the channels, respectively. The parallel view shows long fibroin layers aligned to the freezing direction while the top view of the channels visualizes the micrometer-sized pores. The average pore diameter  $D$  and spacing  $l$  between fibroin layers were calculated from the optical images of cryogels formed at various fibroin concentrations C<sub>SF</sub> (Fig. S2). Fig. 1d shows the variations of  $D$  and  $l$  of cryogels prepared via pre-freezing at −30 and −196 °C plotted against fibroin concentration C<sub>SF</sub>. Both the diameter of the pores and the spacing between fibroin layers corresponding to the width of pore channels decrease as C<sub>SF</sub> is increased. For instance,  $D$  and  $l$  of cryogels prepared using liquid nitrogen as a cold bath decrease from 43 ± 8 to 16 ± 2 μm and from 48 ± 8 to 17 ± 3 μm, respectively, as C<sub>SF</sub> is increased from 2.1 to 16.7 wt%. Moreover, at low C<sub>SF</sub>, cryogels have poly-disperse pores as reflected in Fig. 1d by large error bars whereas the pores become rather uniform as C<sub>SF</sub> is increased. The inverse relation between the pore diameter and C<sub>SF</sub> is likely due to the variation of the water content in the reaction solution. Increasing C<sub>SF</sub> decreases the amount of water developing the ice template in the solution leading to the formation of smaller pores and thinner pore channels. Fig. 1d also shows that  $D$  and  $l$  increase by increasing the cold bath temperature from −196 to −30 °C.

Figs. 2a and b show typical scanning electron micrographs (SEMs) of cryogel scaffolds formed at various C<sub>SF</sub> between 2.1 and 16.7 wt% taken parallel and perpendicular to the freezing direction, respectively. At the lowest concentration of fibroin used (2.1 wt%, left panel), the pores are not stable so that they sandwiched between the fibroin layers whereas at higher concentrations the cryogels possess several hundred micrometers long, aligned fibroin layers interconnected by vertically oriented branches producing a channel-like porous structure. In accord with Fig. 1d, increasing the fibroin concentration C<sub>SF</sub> decreases the size of

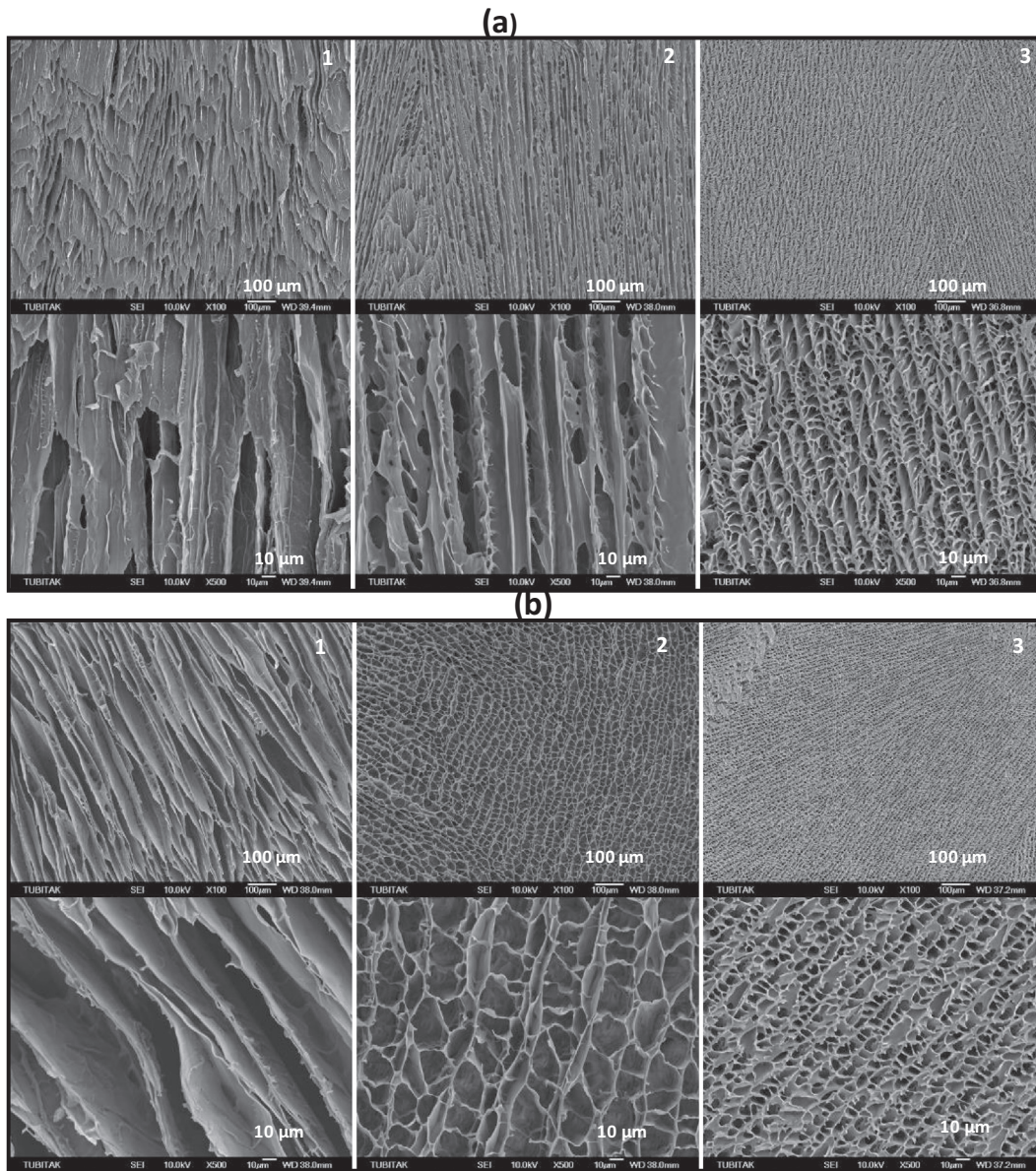


**Fig. 2.** SEM images of cryogel scaffolds formed at  $C_{SF} = 2.1$  (1), 4.2 (2), and 16.7 wt% (3). The images were taken parallel (a) and perpendicular to the freezing direction (b). Scaling bars are 100 μm (upper panel) and 10 μm (bottom panel).

the pores as well as the spacing between the fibroin layers. Fig. 3a, b show SEM images of cryogel scaffolds formed at  $C_{SF} = 8.4$  wt% via freezing at  $-196$  (a) and  $-30$  °C (b). The images were taken perpendicular

to the freezing direction. It is seen that the freezing temperature has an important effect on the pore size. In line with the results obtained from the optical images (Fig. 1d), both the pore diameter and layer spacing

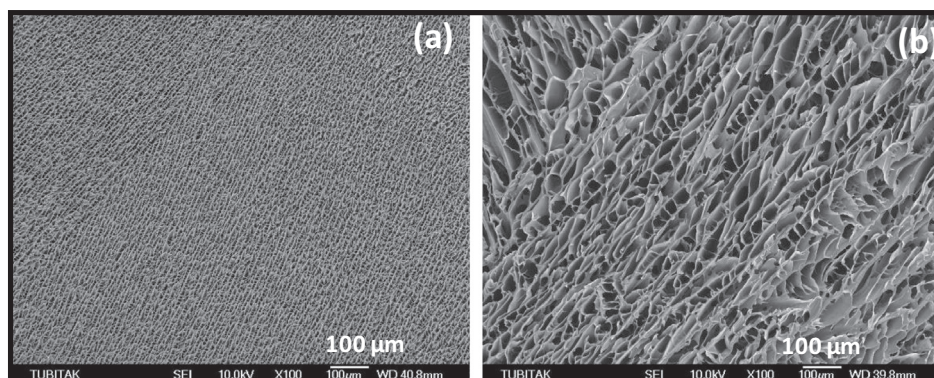


**Fig. 3.** SEM images of cryogel scaffolds formed via freezing at  $-196$  (a) and  $-30$  °C (b).  $C_{SF} = 8.4$  wt%. The images were taken perpendicular to the freezing direction.

increase with increasing temperature of the cold bath. Because the rate of freezing of the reaction solution decreases with increasing cold bath temperature, fewer but larger ice crystals will grow during freezing at a high temperature leading to larger pores [31]. As will be discussed later, cryogels formed via freezing at  $-30\text{ }^{\circ}\text{C}$  exhibit poor mechanical properties as compared to those at  $-196\text{ }^{\circ}\text{C}$ . Therefore, in the following, we will mainly discuss the properties of cryogels prepared via pre-freezing at  $-196\text{ }^{\circ}\text{C}$ .

### 3.2. Water stability of cryogels and possible cryogelation mechanism

All the cryogels were insoluble in water with a gel fraction close to unity revealing that fibroin molecules are completely incorporated into 3D fibroin network. Thermogravimetric analysis (TGA) of freeze-dried gel specimens revealed a weight loss of 5 to 7% at around  $95\text{--}100\text{ }^{\circ}\text{C}$  due to evaporation of bound water and a peak at  $315\text{ }^{\circ}\text{C}$  due to thermal degradation of SF (Fig. S3). DSC scans also show a broad endothermic peak below  $100\text{ }^{\circ}\text{C}$  that disappeared after annealing from  $-50$  to  $250\text{ }^{\circ}\text{C}$  indicating the existence of bound water in freeze-dried cryogel specimens (Fig. S4).

Water-insolubility of the cryogels suggests formation of  $\beta$ -sheets acting as crosslinks by connecting the fibroin chains to a 3D network. FTIR measurements were conducted on freeze-dried fibroin scaffolds to estimate the conformation of SF in the cryogels (for details, see Supporting Information). Fig. 4a shows amide I region of FTIR spectra of SF before (dashed curve) and after cryogelation (blue symbols). A peak at  $1640\text{ cm}^{-1}$  appears before gelation which is typical for random-coil conformation. This peak shifts to  $1620\text{ cm}^{-1}$  and two additional minor peaks at  $1660$  and  $1698\text{ cm}^{-1}$  appear after cryogelation which are attributed to  $\beta$ -sheet,  $\alpha$ -helix and  $\beta$ -turn conformations [37,38]. Fibroin conformation in the cryogels was estimated via peak separation of amide I band by selecting a Gaussian model for curve fitting [33,34]. The hidden peaks after peak separation shown in Fig. 4a by thin gray curves with peak positions at  $1620$ ,  $1640$ ,  $1660$ , and  $1698\text{ cm}^{-1}$ , corresponding to  $\beta$ -sheet, random-coil,  $\alpha$ -helix, and  $\beta$ -turn conformations, respectively, were used to estimate the conformation of fibroin network chains. Fig. 4b shows conformations of fibroin in cryogels plotted against fibroin concentration  $C_{\text{SF}}$ , where the data at  $C_{\text{SF}} = 0\%$  correspond to fibroin before gelation. It is seen that the content of  $\alpha$ -helix decreases in favor of the random coil and  $\beta$ -sheet contents and the fraction of  $\beta$ -sheets increases from  $14 \pm 3$  to  $32 \pm 1\%$  after cryogelation which is, within the limits of experimental error, independent of fibroin concentration.

Formation of water-insoluble fibroin scaffolds with an aligned porous structure can be explained using the following scenario: Upon immersion of the bottom part of the reactor into cold bath, ice crystals start to grow in down-to-up direction during which the solutes silk fibroin (SF), BDDE, and TEMED are expelled from the ice and they concentrate in the unfrozen domains of the reaction solution. This leads to the formation of a highly concentrated solution of SF, BDDE, and TEMED surrounding the directionally growing ice crystals. After thermal equilibrium of the reaction system with the cold bath at  $-196\text{ }^{\circ}\text{C}$ , the completely frozen system consists of two phases, namely frozen solution phase containing all the reactants, and pure ice crystal phase aligned to the freezing direction. Upon heating to  $-18\text{ }^{\circ}\text{C}$  to conduct the cryogelation reactions, frozen solution phase containing all solutes will partially melt to attain thermal equilibrium with the cryostat temperature of  $-18\text{ }^{\circ}\text{C}$ . It was reported that when an aqueous solution containing 6 wt% SF is cooled to  $-18\text{ }^{\circ}\text{C}$ , at thermal equilibrium it consists of 88 wt% ice and the rest being an unfrozen solution containing 37 wt% fibroin [34]. This process, called cryoconcentration is due to the high solute concentration preventing the freezing of the whole system [31]. Thus, during the incubation period at  $-18\text{ }^{\circ}\text{C}$ , cryogelation in unfrozen fibroin channels containing BDDE and TEMED leads to the formation of a 3D fibroin network filled with ice template forming pores after melting at room temperature. Previous work shows that the amine groups on fibroin molecules are responsible for the crosslinking reactions of fibroin with diepoxide crosslinkers such as BDDE [33]. Introduction of BDDE crosslinks between fibroin molecules decreases the mobility of the chains, which triggers the conformational transition from random-coil to  $\beta$ -sheet structure and hence fibroin gelation [33,34]. The occurrence of gelation reactions at such a low temperature is due to the cryoconcentration phenomenon producing a high concentration of reactants. Thus, decreasing the reaction rate due to low temperature is compensated by the increasing concentration of the reactants.

### 3.3. Swelling anisotropy and swollen state porosity of cryogels

To highlight the effect of the microstructural anisotropy on the swelling behavior of the cryogels, we conducted swelling measurements both parallel and perpendicular to the freezing direction. The degree of volume swelling was determined by measuring the lengths of the gel specimens in directions parallel  $l_x$  and perpendicular to the freezing direction  $l_y$  (Fig. 5a). Volume swelling ratios in these directions denoted by  $q_{v,x}$  and  $q_{v,y}$ , respectively, were calculated as  $q_{v,x} = (l_x / l_{x,0})^3$  and  $q_{v,y} = (l_y / l_{y,0})^3$ , where the subindex  $o$  denotes the initial sample

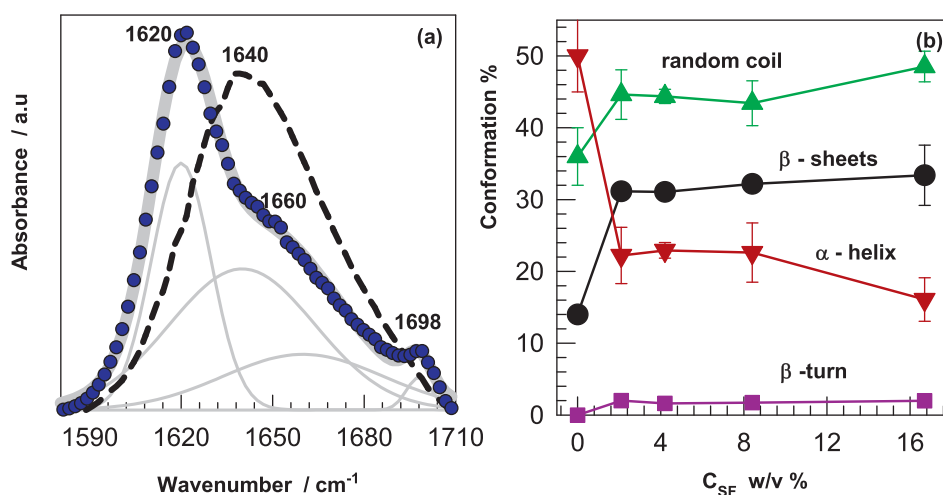


**Fig. 4.** (a): Typical ATR-FTIR spectra of freeze-dried silk fibroin sample before (dashed curve) and after cryogelation at  $C_{\text{SF}} = 8.4\text{ wt}\%$  (filled blue circles). The result of curve fitting for the original spectrum after cryogelation is shown by the thick gray curve. The thin gray curves represent the hidden peaks after peak separation with peak positions at  $1620$ ,  $1640$ ,  $1660$ , and  $1698\text{ cm}^{-1}$ . (b): Fractions of random coil,  $\beta$ -sheet,  $\alpha$ -helix and  $\beta$ -turn conformations in cryogels plotted against  $C_{\text{SF}}$ .

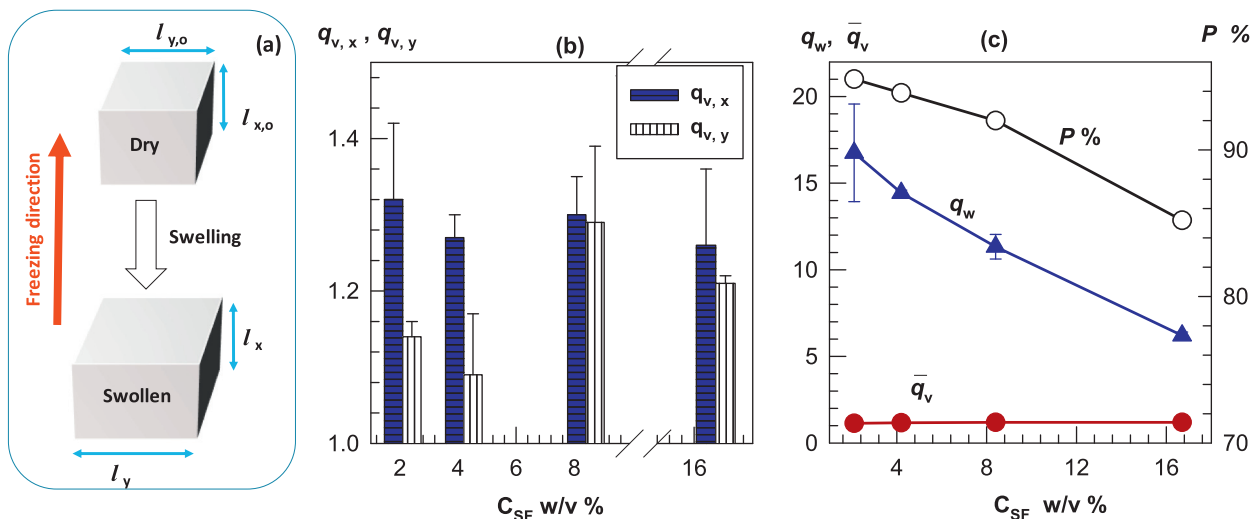


**Fig. 5.** (a): Cartoon showing swelling of gel specimen along parallel and perpendicular to the freezing direction. (b): The volume swelling ratio of cryogels measured parallel  $q_{v,x}$  and perpendicular to the freezing direction  $q_{v,y}$  plotted against  $C_{SF}$ . (c): The weight  $q_w$  and volume swelling ratios  $\bar{q}_v$  of cryogels and their swollen state porosities  $P$  plotted against  $C_{SF}$ .

length in dry state. Fig. 5b compares  $q_{v,x}$  and  $q_{v,y}$  ratios of cryogels formed at various fibroin concentrations  $C_{SF}$ . All cryogels exhibit a larger degree of swelling in the  $x$ -direction, that is, parallel to the freezing direction, as compared to the  $y$ -direction. This could be related to the pore channels in the cryogels aligned to the freezing ( $x$ -) direction so that the expansion of the sample in water occurs in the same direction rather than the radial direction. Moreover, the swelling anisotropy calculated as  $q_{v,x}/q_{v,y}$  decreases as fibroin concentration is increased, and the largest swelling anisotropy of  $1.17 \pm 0.02$  was observed at  $C_{SF} = 4.2$  wt%.

In Fig. 5c, the average of the volume swelling ratios in both direction  $\bar{q}_v$  together with the weight swelling ratio  $q_w$  of the cryogels are plotted against the fibroin concentration  $C_{SF}$ . The average volume swelling ratio  $\bar{q}_v$  of all cryogels is  $1.2 \pm 0.1$ , whereas the weight swelling ratio  $q_w$  is between 14 and 21, and it increases as  $C_{SF}$  is decreased. Because the volume expansion of gels is related to their crosslink density, the low degree of volume swelling indicates highly crosslinked structure of fibroin network, i.e., pore walls, restricting its expansion due to the favorable mixing entropy effect. A much larger weight swelling as compared to the volume swelling is due to the interconnected open pores that are filling and emptying during swelling and drying, respectively, without changing much the gel volume. Swollen state porosity can be calculated from the swelling ratios as  $P = 1 - \bar{q}_v [1 + (q_w - 1)\rho]^{-1}$  where  $\rho$  is the fibroin density (1.35 g/mL) [39]. Open symbols in Fig. 5c showing porosities reveal that all cryogels are highly porous and the porosity decreases from 96 to 85% with increasing fibroin concentration.

### 3.4. Viscoelasticity of cryogels

Viscoelastic properties of the cryogels were investigated by oscillatory deformation tests at a strain amplitude  $\gamma_0$  of 1%, which is in the linear regime of the cryogels (Fig. S5). Figs. 6a, b show the storage modulus  $G'$  and loss factor  $\tan \delta$  of the cryogels formed at various  $C_{SF}$  plotted against the frequency  $\omega$ . Both  $G'$  and  $\tan \delta$  exhibit weak frequency dependencies reflecting the elastic nature of the cryogels. The modulus  $G'$  increases from  $\sim 1$  to  $\sim 50$  kPa with increasing  $C_{SF}$  due to the simultaneous increase of the  $\beta$ -sheet amount in unit volume of cryogel. Moreover, the loss factor  $\tan \delta$  is above 0.1 for all cryogels, which is around one order of magnitude larger than that of nonporous fibroin hydrogels [33]. Because  $\tan \delta$  is a measure of energy dissipation, this suggests a larger extent of energy dissipation in cryogels as compared to hydrogels. This behavior is likely due to the squeezability of fibroin cryogels which

is comparable to squeezing out a sponge. The images in Fig. 6c demonstrate a macroscopic visualization of this behavior for a cryogel specimen formed at  $C_{SF} = 16.7$  wt%. The specimen could be compressed by a strain  $\varepsilon$  of 80% and, upon unloading, it recovers its original shape immediately by soaking up the released water back into its pores. Similar to this macroscopic view, within each cycle of the oscillatory deformation tests, pore walls of fibroin cryogel approach each other and move away again, during which the pore water is squeezed out and soaked up back. This creates viscous stresses and energy dissipation as reflected by increased loss modulus and hence loss factor as compared to nonporous fibroin gels having the same storage modulus [33].

To further demonstrate the energy dissipation, cyclic strain-sweep tests between strain amplitudes  $\gamma_0$  1% and 1000% were conducted at a fixed frequency of  $6.28 \text{ rad s}^{-1}$ . The results are shown in Fig. 6d where  $G'$  (filled symbols) and the loss modulus  $G''$  (open symbols) are plotted against strain  $\gamma_0$ . Results of up and down strain sweep tests are shown by circles and triangles, respectively. An apparent gel-to-sol transition occurs at around 10% strain and the cryogel behaves like a liquid with a loss factor of around 6 at 1000% strain. This transition is reversible, that is, if the strain is reduced back to 1%, the cryogel recovers its initial viscoelastic properties. We can explain this unusual behavior with the squeezability of the cryogels. As depicted in the inset to Fig. 6d, as the strain is increased at a fixed frequency, pore water is gradually squeezing out of the cryogel forming a water layer between the gel phase and the upper plate of the rheometer. Thus, the released water instead of the densified cryogel is measured at high strains while reducing the strain results soaking up water back into the gel sample so that the initial properties are recovered.

### 3.5. Mechanical anisotropy of cryogels

Figs. 7a, b show representative stress-strain curves of cryogels formed at  $C_{SF} = 8.4$  and 16.7 wt%, respectively, in dry (left panel) and swollen states (right panel). As illustrated in the inset images, the measurements were performed along parallel (solid curves) and perpendicular to the freezing direction (dotted curves). Comparing the results in both directions, the cryogels exhibit a higher stiffness in the parallel direction at a small strain, whereas the difference observed between parallel and perpendicular directions vanishes at large strains. Moreover, stress-strain curves of both dry and swollen cryogels can be divided into three zones:

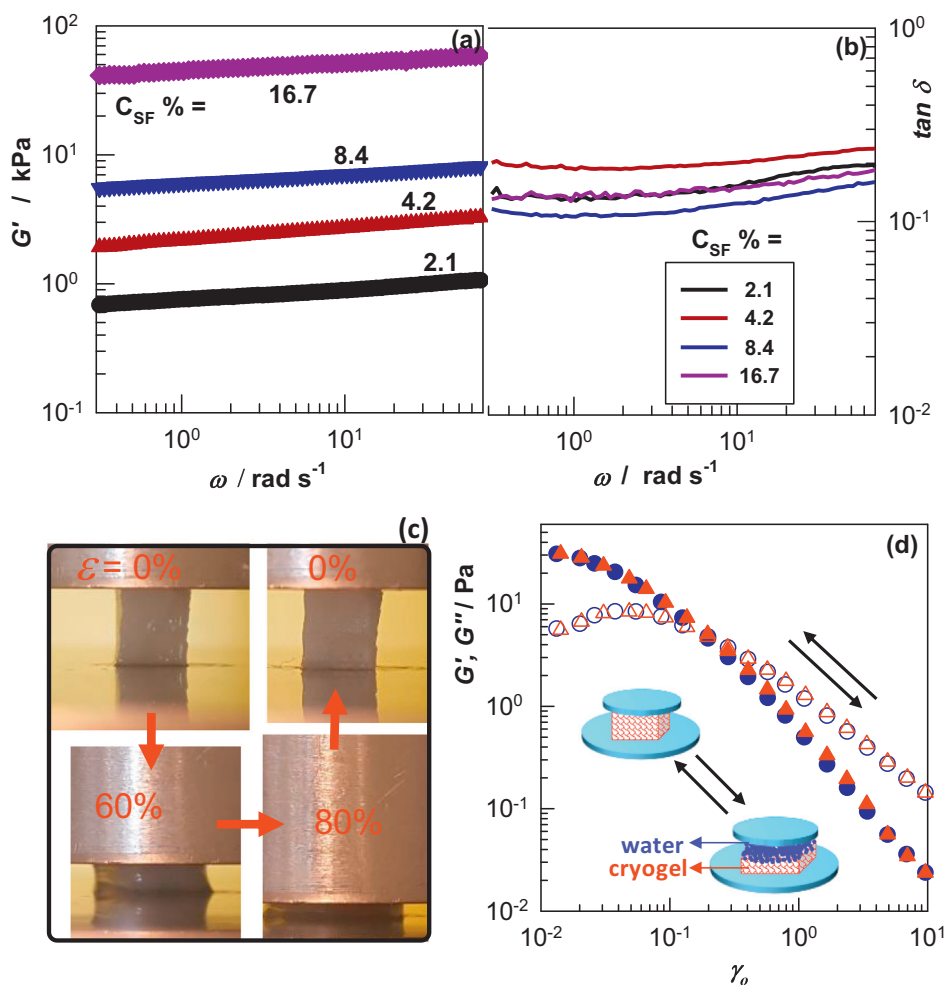


**Fig. 6.** (a, b): Storage modulus  $G'$  (a) and loss factor  $\tan \delta$  (b) of the cryogels plotted against frequency  $\omega$ . Strain amplitude  $\gamma_0 = 1\%$ . Fibroin concentrations  $C_{SF}$  (in wt%) are indicated. (c): Images of a cryogel specimen during uniaxial compression up to a strain  $\varepsilon$  of 80% followed by unloading to zero strain during which the sample soaks up the squeezed water back into its pores. (d):  $G'$  (filled symbols) and loss modulus  $G''$  (open symbols) of the cryogels formed at  $C_{SF} = 16.7$  wt% plotted as a function of strain  $\gamma_0$  at  $\omega = 6.28$  rad  $s^{-1}$ . Results of up and down strain sweep tests are shown by circles and triangles, respectively. Temperature = 25 °C. The cartoon in the inset shows formation of a water layer between the gel phase and the upper plate of the rheometer at high strains.

- (i) Elastic region up to a strain of about 10% during which stress linearly increases with strain,
- (ii) Plateau region between 10 and 60% strains during which the cryogel easily deforms, and
- (iii) Densification region above 60% strain.

The elastic region is expected for any porous or nonporous elastic material at small strains and indicates that the pore walls of the cryogel remain stable. In the following, this regime was characterized by Young's modulus  $E$  calculated from the slope of the curves between 2 and 4% compressions, and the compressive stress  $\sigma_{comp}$  which is the stress at 3% strain. In the second region, the fibroin channels building the porous structure of cryogels start to collapse by elastic buckling and continues until the majority of them have done so. As a consequence, the cryogel easily deforms in the plateau region due to squeezing out air or pore water for dry and swollen cryogels, respectively. This region was characterized by the plateau stress  $\sigma_p$ , which is a measure of the mechanical stability of the porous structure. Fig. 7c showing the dependence of the plateau stress  $\sigma_p$  of dried cryogels on the fibroin concentration  $C_{SF}$  in directions parallel (circles) and perpendicular (triangles) to the freezing direction reveals that  $\sigma_p$  is larger in parallel direction and it increases from  $10^{-2}$ – $10^{-1}$  to  $10^0$  MPa with increasing  $C_{SF}$  from 2.1 to 16.7 wt% reflecting increasing mechanical stability of the porous structure at high fibroin concentration. However, swelling

of cryogels decreases the plateau stress  $\sigma_p$  and the plateau becomes less visible due to the glassy-to-rubbery state transition in fibroin network. In the final densification regime, most of the air or pore water in the cryogel is squeezed out so that a nearly nonporous fibroin network is compressed, as manifested by an upward growth of stress (strain-hardening). Because of the disappearance of the pores in this regime, stress-strain curves recorded parallel and perpendicular to the freezing direction approach each other and similar ultimate properties were obtained. This is also illustrated in Fig. 7d showing the fracture stress  $\sigma_f$  of dry and swollen cryogels measured at two directions plotted against  $C_{SF}$ .  $\sigma_f$  slightly increases with  $C_{SF}$  and no directional dependence is observable over the whole range of fibroin concentration.

Fig. 8a, b show  $C_{SF}$  dependences of Young's modulus  $E$  (upper panel) and compressive stress  $\sigma_{comp}$  (bottom panel) of dry and swollen cryogels, respectively, measured along parallel (circles) and perpendicular to the freezing direction (triangles). In both directions, increasing fibroin concentration  $C_{SF}$  improves the mechanical performance of cryogels both in their dry and swollen states. The modulus  $E$  and compressive stress  $\sigma_{comp}$  in the parallel direction are much higher than those in the perpendicular direction. For instance, at  $C_{SF} = 16.7$  wt% the moduli  $E_{\parallel}$  and  $E_{\perp}$  are  $18 \pm 3$  and  $5.8 \pm 0.3$  MPa, respectively. Moreover, the difference in the modulus becomes larger with increasing  $C_{SF}$ . Fig. 8c, d show the anisotropies in modulus, compressive stress  $\sigma_{comp}$ ,

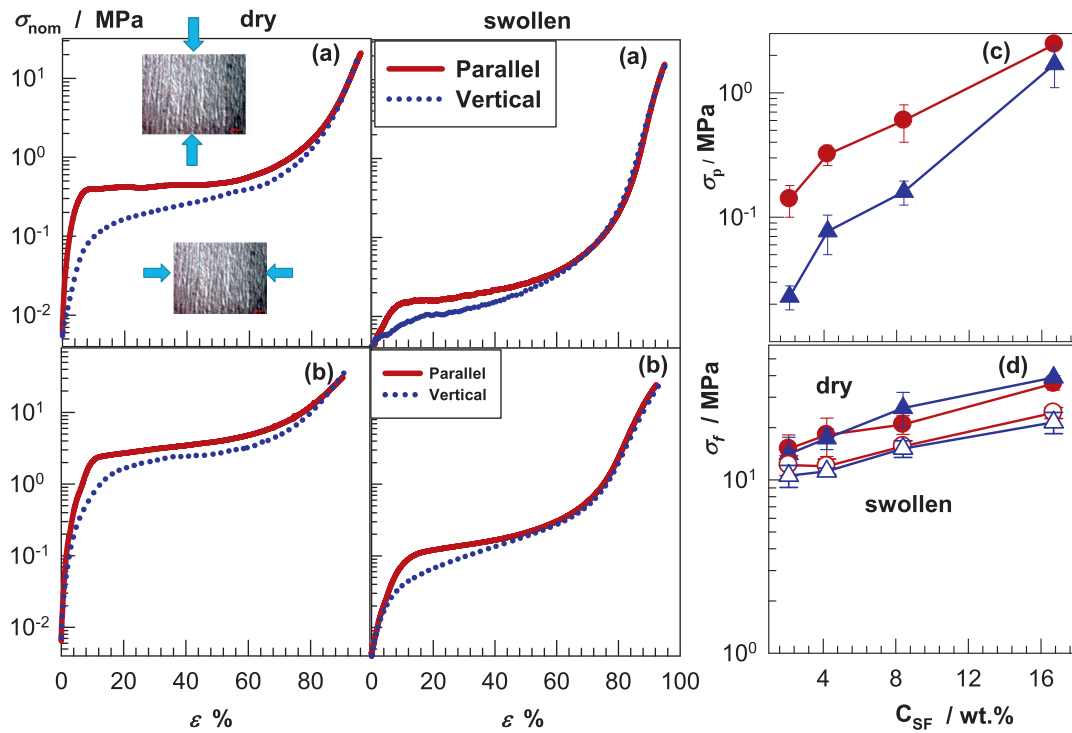


**Fig. 7.** (a, b): Compressive stress-strain curves of cryogels formed at  $C_{SF} = 8.4$  (a) and  $16.7$  wt% (b) in dry (left panel) and swollen states (right panel). Uniaxial compression tests were performed parallel (solid curves) and perpendicular to the freezing direction (dotted curves). (c, d): Plateau stress  $\sigma_p$  (c) and fracture stress  $\sigma_f$  (d) of cryogels measured in parallel (circles) and perpendicular to the freezing direction (triangles) plotted against the fibroin concentration  $C_{SF}$ . The  $\sigma_p$  data are from dried cryogel samples while  $\sigma_f$  data are from dried (filled symbols) and swollen cryogels (open symbols).

and fracture stress  $\sigma_f$  of dry and swollen cryogels, respectively, plotted against  $C_{SF}$ . The anisotropy in the fracture stress is close to unity revealing the isotropic behavior of cryogels at large strains whereas both the modulus and compressive stress show directional dependences. In dry state, the maximum degree of anisotropy in the modulus  $E_{||}/E_{\perp}$  is  $21 \pm 5$  which was observed at the lowest fibroin concentration (2.1 wt%),

i.e.,  $E_{||} = 2.3 \pm 0.5$  MPa and  $E_{\perp} = 0.11 \pm 0.03$  MPa. This value is the highest modulus anisotropy reported so far in the literature. The anisotropy in the compressive stress also attains a maximum value of  $7 \pm 2$  at 2.1 wt% fibroin. In swollen state, the maximum modulus and compressive stress anisotropies are  $8 \pm 2$  and  $1.9 \pm 0.5$ , respectively, observed at 4.2 wt%  $C_{SF}$ .

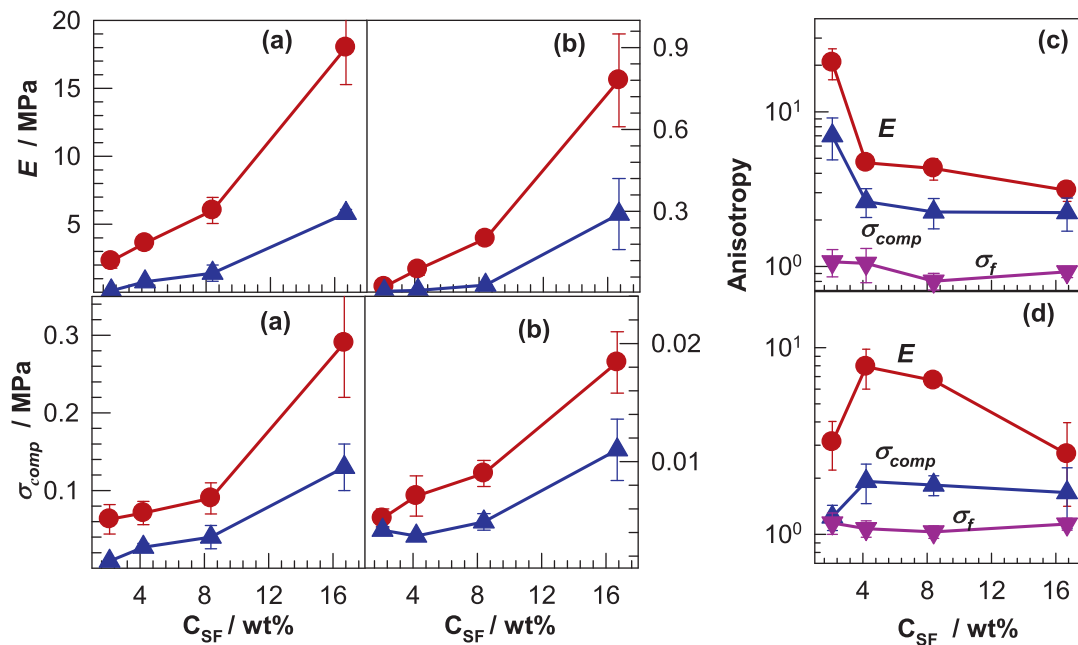


**Fig. 8.** (a, b): Young's modulus  $E$  (upper panel) and compressive stress  $\sigma_{comp}$  (bottom panel) of dried (a) and swollen cryogels (b) measured in parallel (circles) and perpendicular to the freezing direction (triangles) plotted against fibroin concentration  $C_{SF}$ . (c, d): Anisotropies in modulus  $E$ , compressive stress  $\sigma_{comp}$ , and fracture stress  $\sigma_f$  of dry (c) and swollen cryogels (d) plotted against fibroin concentration  $C_{SF}$ .

As mentioned in the experimental part, Young's modulus  $E$  of the cryogels was calculated from the slope of the stress-strain curves between 2 and 4% strains. Detailed calculations revealed that the slope of the curves continuously varies even in the elastic region. For instance, Fig. 9a shows stress-strain curves of fibroin cryogels formed at various SF concentrations up to a strain of 10%. The measurements were conducted along parallel (solid curves) and perpendicular to the freezing direction (dashed curves). From these curves the instantaneous moduli  $E_i$  was calculated as the slope between two consecutive data points and plotted against the strain  $\varepsilon$  in Fig. 9b. To eliminate noise in the data series, they were smoothed using the negative exponential procedure with a sampling proportion of 0.4, i.e., 10 data points for 4 smoothed values (Fig. S6) [40]. The solid circles in Fig. 9b show Young's moduli  $E$  of the cryogels. It is seen that, similar to the cancellous bone [41], all fibroin scaffolds exhibit peak moduli at a critical strain which are larger than their Young's moduli  $E$ . For instance,  $E_i$  of the cryogel formed at  $C_{SF} = 16.7$  wt% is 45 MPa which is about 2.5-fold larger than its Young's modulus. Moreover, the modulus anisotropy at the peak position, i.e., the  $E_{i\parallel}/E_{i\perp}$  ratio is also larger than that calculated from Young's modulus as  $E_{\parallel}/E_{\perp}$ . For instance,  $E_{i\parallel}/E_{i\perp}$  and  $E_{\parallel}/E_{\perp}$  ratios are  $3.1 \pm 0.5$  and  $5.4 \pm 0.3$ , respectively, for the cryogels formed at  $C_{SF} = 16.7$  wt%.

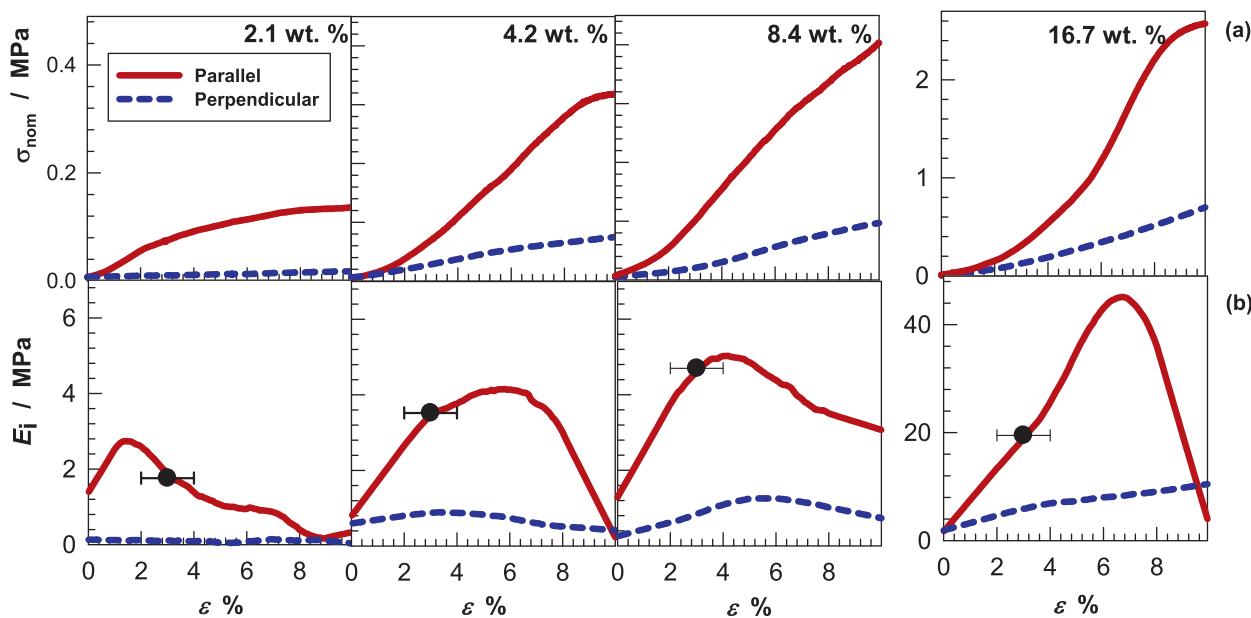
### 3.6. Mechanism of energy dissipation

Cyclic mechanical tests are a mean to investigate the anisotropy in viscous energy dissipation of the cryogels. We conducted uniaxial compression tests at a strain rate of  $0.3 \text{ mm min}^{-1}$  up to a maximum strain  $\varepsilon_{\max}$  followed by unloading at the same rate to zero strain. This loading/unloading cycle was successively repeated with a waiting time of 5 min between the cycles during which a few drops of water was added to the gel specimen to eliminate water loss by evaporation. Fig. 10a, b show typical stress-strain curves from four successive cyclic compression tests to a fixed maximum strain  $\varepsilon_{\max}$  of 80% (a) and with increasing  $\varepsilon_{\max}$  from 20 to 80% are shown (b). The tests were conducted parallel to the freezing direction on the cryogels formed at  $C_{SF} = 4.2$  wt%. The loading and unloading curves are shown by the solid and dotted lines, respectively. The general trend is that the unloading curves follow a different path from the loading ones revealing energy dissipation during the mechanical cycles. Moreover, each loading curve follows previous

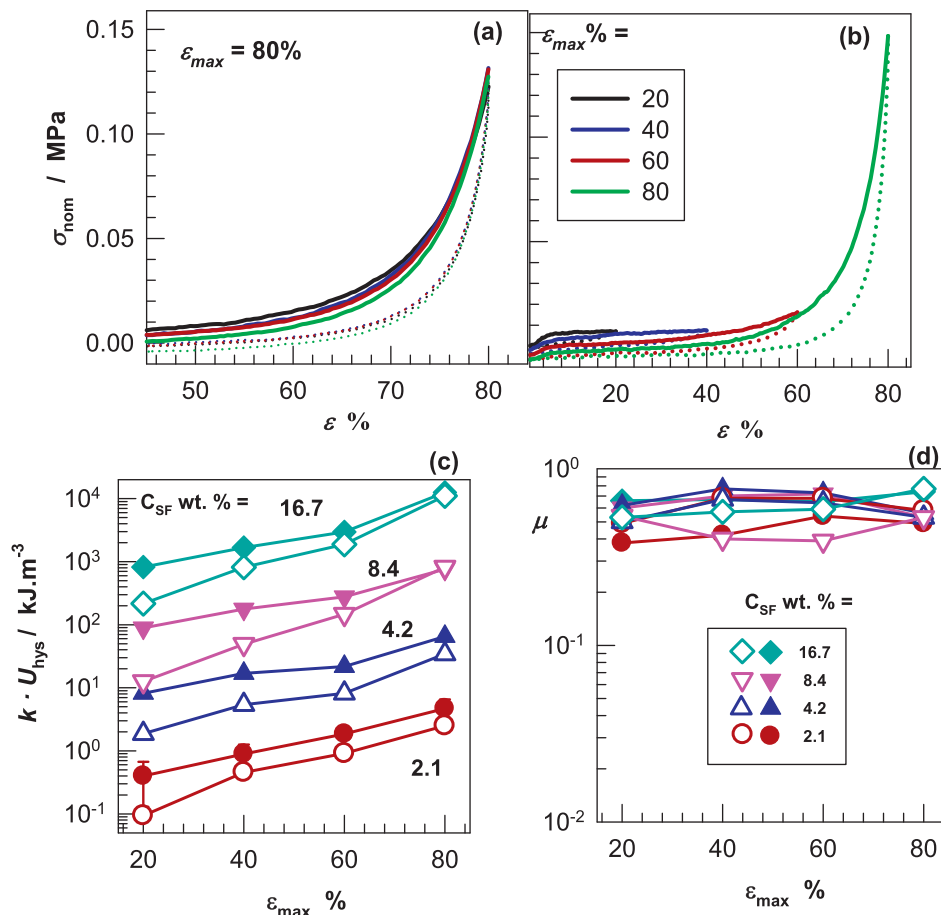
loading indicating that the cycles are reversible, i.e., the original microstructure of the cryogel is recovered after the cycle. This is an indication of self-recoverability of fibroin cryogels, as also illustrated in Fig. 6c showing a macroscopic visualization of this behavior. Indeed, for  $\varepsilon_{\max} = 80\%$  the dissipated (hysteresis) energy  $U_{\text{hys}}$  calculated from the area between loading and unloading curves is independent on the number of cycles and equals to  $4 \pm 1 \text{ kJ m}^{-3}$ .

Fig. 10c shows the hysteresis energies  $U_{\text{hys}}$  of the cryogels formed at various fibroin concentrations  $C_{SF}$  plotted against the maximum strain  $\varepsilon_{\max}$ .  $U_{\text{hys}}$  data were calculated from cyclic mechanical tests conducted parallel (filled symbols) and perpendicular to the freezing direction (open symbols). For the sake of clarity, the data were vertically shifted by a factor  $k$ . It is seen that at small maximum strains  $\varepsilon_{\max}$ ,  $U_{\text{hys}}$  is about one order of magnitude larger in the parallel direction reflecting larger viscous energy dissipation as compared to the perpendicular direction. The directional dependence of  $U_{\text{hys}}$  decreases with increasing strain and disappears at  $\varepsilon_{\max} = 80\%$ . This finding is in accord with the mechanical test results given in Fig. 7 showing that the ultimate properties of cryogels are almost independent of direction.

We can explain the above results with the friction-induced energy dissipation in the cryogels. Because of the squeezability of the cryogels, high friction between fibroin pore walls can be produced when water moves through the pores, as reported previously [42]. Thus, the friction seems to be a primary factor responsible for the energy dissipation. According to the Amonton's law, frictional force  $F$  between two solids is related to the load  $W$  forcing them together by  $F = \mu W$  where  $\mu$  is the frictional coefficient and is generally between 0.5 and 1.0 [43]. Although the frictional behavior of hydrogels deviates from the Amonton's law [44], swelling of fibroin cryogels mainly occurs by filling of the pores with water rather than volume swelling, and the pore walls absorb only 20% water to attain the equilibrium state (Fig. 5c). Thus, fibroin pore walls of cryogels are solid-like as compared to highly swollen hydrogels. Moreover, the ratio of dissipated energy to the loading energy, that is, the amount of energy dissipated per energy given can be regarded as the frictional coefficient  $\mu$ , which should be independent of  $C_{SF}$ , or the direction of the measurements. By dividing  $U_{\text{hys}}$  to the area under the loading curve, we calculated  $\mu$  for all hydrogels and plotted against  $\varepsilon_{\max}$  in Fig. 10d. It is seen that the  $\mu$  is indeed independent on the direction of the measurements, or fibroin concentration  $C_{SF}$ , and it



**Fig. 9.** Stress-strain curves up to a strain of 10% (a) and instantaneous modulus  $E_i$  of the cryogels (b) plotted against the strain  $\varepsilon$ . Solid and dashed curves are the results obtained from parallel and perpendicular to the freezing direction, respectively. The symbols represent the Young's modulus of the cryogels and the vertical bars indicate the range between 2 and 4% strain where the modulus was calculated.



**Fig. 10.** (a, b): Nominal stress  $\sigma_{nom}$  vs elongation ratio  $\epsilon$  curves from cyclic compression tests of swollen cryogels conducted parallel to the freezing direction. C<sub>SF</sub> = 4.2 wt%. Four successive cycles to a maximum strain  $\epsilon_{max} = 80\%$  (a) and with increasing  $\epsilon_{max}$  from 20 to 80% are shown (b). Temperature =  $24 \pm 1$  °C. (c): Hysteresis energies  $U_{hys}$  calculated from the cyclic test results shown as a function of  $\epsilon_{max}$ . The measurements were conducted parallel (filled symbols) and perpendicular to the freezing direction (open symbols). For the sake of clarity, the data were vertically shifted by a factor  $k$ , which is 1, 10, 70, and 60 for C<sub>SF</sub> = 2.1, 4.2, 8.4, and 16.7 wt%, respectively. (d): Dissipated energy  $\mu$  per loading energy in parallel (filled symbols) and perpendicular directions (open symbols) plotted against  $\epsilon_{max}$ .

equals to  $0.6 \pm 0.1$ . Thus, around 60% of the energy given to the cryogels are dissipated due to the friction between the pore walls. Because creating an effective energy dissipation mechanism is the main technique for toughness improvement in hydrogels [2], the large friction-induced energy dissipation in cryogels is responsible for their almost complete squeezability and self-recoverability.

The results summarized above were obtained by directional freezing of the gelation solution at  $-196$  °C followed by cryogelation at  $-18$  °C to obtain fibroin cryogels. Increasing the cryogelation temperature from  $-18$  to  $-6$  °C resulted in no change in the mechanical properties as well as in the degree of anisotropy in the cryogels (Fig. S7). However, conducting the initial directional freezing process at  $-30$  °C in ethylene glycol/water mixture instead of  $-196$  °C slightly deteriorated the mechanical properties of the cryogels (Fig. S7). This could be related to the formation of larger pores due to the slower rate of freezing of the solution at  $-30$  °C as shown in Figs. 1d and 3, leading to a decrease in the mechanical performance of the cryogels.

#### 4. Conclusions

A novel directional freezing/cryogelation method was described for fabrication of high-strength and rapid self-recoverable silk fibroin scaffolds with anisotropic properties. Significant anisotropies in the micro-structure, swelling, and mechanical properties were achieved that could be tuned by the silk fibroin concentration. By adjusting the synthesis parameters, we were able to create fibroin scaffolds exhibit the highest modulus anisotropy so far reported,  $21 \pm 5$ , with moduli  $E =$

$2.3 \pm 0.5$  and  $0.11 \pm 0.03$  MPa measured along parallel and perpendicular to the freezing direction, respectively. Although the cryogels exhibit solid-like behavior with a weak frequency dependent storage modulus, they undergo gel-to-sol transition at around 10% strain, which is attributed to their squeezability creating viscous stresses and energy dissipation. Stress-strain curves of cryogels reveal the existence of two phases: The low-strain phase in which the fibroin micro-channels are mostly straight, i.e., pore walls are stable, and a high-strain phase in which the micro-channels are mostly buckled so that the pores are disappeared. The transition between the two phases occurs over the plateau regime during which water is squeezed out easily. Cyclic mechanical tests reveal that the friction between the fibroin pore walls is the primary factor responsible for the energy dissipation. Independent on the fibroin concentration or direction of the measurements, 60% of the mechanical energy given to the cryogels are dissipated due to the friction which is responsible for their almost complete squeezability and self-recoverability.

#### Acknowledgments

O. O. thanks Turkish Academy of Sciences (TUBA) for the partial support.

#### Appendix A. Supplementary data

Supplementary data to this article can be found online at <https://doi.org/10.1016/j.ijbiomac.2018.09.087>.

## References

- [1] P. Calvert, Hydrogels for soft machines, *Adv. Mater.* 21 (2009) 743–756.
- [2] C. Creton, 50th anniversary perspective: networks and gels: soft but dynamic and tough, *Macromolecules* 50 (2017) 8297–8316.
- [3] K. Sano, Y. Ishida, T. Aida, Synthesis of anisotropic hydrogels and their applications, *Angew. Chem. Int. Ed.* 57 (2018) 2–14.
- [4] L.N. Williams, S.H. Elder, J.L. Bouvard, M.F. Horstemeyer, The anisotropic compressive mechanical properties of the rabbit patellar tendon, *Biorheology* 45 (2008) 577–586.
- [5] D.M. Elliott, L.A. Setton, Anisotropic and inhomogeneous tensile behavior of the human annulus fibrosus: experimental measurement and material model predictions, *J. Biomech. Eng.* 123 (2001) 256–263.
- [6] A. Argun, U. Gulyuz, O. Okay, Interfacing soft and hard materials with triple-shape-memory and self-healing functions, *Macromolecules* 51 (2018) 2437–2446.
- [7] K. Kaneda, K. Uematsu, H. Masunaga, Y. Tominaga, K. Shigehara, K. Shikina, Flow-orientation of internal structure and anisotropic properties on hydrogels consisted of imogolite hollow nanofibers, *Sen'i Gakkaishi* 70 (2014) 137–144.
- [8] Y. Tanaka, A. Kubota, M. Matsusaki, T. Duncan, Y. Hatakeyama, K. Fukuyama, A.J. Quantock, M. Yamato, M. Akashi, K. Nishida, Anisotropic mechanical properties of collagen hydrogels induced by uniaxial-flow for ocular applications, *J. Biomater. Sci. Polym. Ed.* 22 (2011) 1427–1442.
- [9] L.E. Millon, H. Mohammadi, W.K. Wan, Anisotropic polyvinyl alcohol hydrogel for cardiovascular applications, *J. Biomed Mater Res B Appl Biomater* 79 (2006) 305–311.
- [10] W. Yang, H. Furukawa, J.P. Gong, Highly extensible double-network gels with self-assembling anisotropic structure, *Adv. Mater.* 20 (2008) 4499–4503.
- [11] J. Wu, Q. Zhao, J. Sun, Q. Zhou, Preparation of poly(ethylene glycol) aligned porous cryogels using a unidirectional freezing technique, *Soft Matter* 8 (2012) 3620–3626.
- [12] H. Zhang, A.I. Cooper, Aligned porous structures by directional freezing, *Adv. Mater.* 19 (2007) 1529–1533.
- [13] H. Zhang, I. Hussain, M. Brust, M.F. Butler, S.P. Rannard, A.I. Cooper, Aligned two- and three-dimensional structures by directional freezing of polymers and nanoparticles, *Nat. Mater.* 4 (2005) 787–793.
- [14] W. Wan, A.D. Bannerman, L. Yang, H. Mak, Poly (vinyl alcohol) cryogels for biomedical applications, *Adv. Polym. Sci.* 263 (2014) 283–321.
- [15] S. Chatelin, M. Bernal, T. Deffieux, C. Papadacci, P. Flaud, A. Nahas, C. Boccara, J.L. Gennisson, M. Tanter, M. Pernot, Anisotropic polyvinyl alcohol hydrogel phantom for shear wave elastography in fibrous biological soft tissue: a multimodality characterization, *Phys. Med. Biol.* 59 (2014) 6923–6940.
- [16] C.M. Voge, M. Kariolis, R.A. MacDonald, J.P. Stegemann, Directional conductivity in SWNT-collagen-fibrin composite biomaterials through strain-induced matrix alignment, *J. Biomed. Mater. Res. A* 86 (2008) 269–277.
- [17] A. Osorio-Madrado, M. Eder, M. Rueggeberg, J.K. Pandey, M.J. Harrington, Y. Nishiyama, J.L. Putaux, C. Rochas, I. Burgert, Reorientation of cellulose nanowhiskers in agarose hydrogels under tensile loading, *Biomacromolecules* 13 (2012) 850–856.
- [18] M.C. Swan, D.G. Bucknall, T.E. Goodacre, J.T. Czernuszka, Synthesis and properties of a novel anisotropic self-inflating hydrogel tissue expander, *Acta Biomater.* 7 (2011) 1126–1132.
- [19] M. Haque, G. Kamita, T. Kurokawa, K. Tsujii, J.P. Gong, Unidirectional alignment of lamellar bilayer in hydrogel: one-dimensional swelling, anisotropic modulus, and stress/strain tunable structural color, *Adv. Mater.* 22 (2010) 5110–5114.
- [20] X. Pei, T. Zan, H. Li, Y. Chen, L. Shi, Z. Zhang, Pure anisotropic hydrogel with an inherent chiral internal structure based on the chiral nematic liquid crystal phase of rod-like viruses, *ACS Macro Lett.* 4 (2015) 1215–1219.
- [21] C. Vepari, D.L. Kaplan, Silk as a biomaterial, *Prog. Polym. Sci.* 32 (2007) 991–1007.
- [22] F. Vollrath, D. Porter, Silks as ancient models for modern polymers, *Polymer* 50 (2009) 5623–5632.
- [23] J.G. Hardy, L.M. Romer, T.R. Scheibel, Polymeric materials based on silk proteins, *Polymer* 49 (2008) 4309–4327.
- [24] J. Melke, S. Midha, S. Ghosh, K. Ito, S. Hofmann, Silk fibroin as biomaterial for bone tissue engineering, *Acta Biomater.* 31 (2016) 1–16.
- [25] A.C. Paz, J. Soleas, J.C. Poon, D. Trieu, T.K. Waddell, A.P. McGuigan, Challenges and opportunities for tissue-engineering polarized epithelium, *Tissue Eng. B Rev.* 20 (2014) 56–72.
- [26] M. Barrow, A. Eltmimi, A. Ahmed, P. Myers, H. Zhang, Frozen polymerization for aligned porous structures with enhanced mechanical stability, conductivity, and as stationary phase for HPLC, *J. Mater. Chem.* 22 (2012) 11615–11620.
- [27] M.C. Asuncion, J.C. Goh, S.L. Toh, Anisotropic silk fibroin/gelatin scaffolds from unidirectional freezing, *Mater. Sci. Eng. C Mater. Biol. Appl.* 67 (2016) 646–656.
- [28] Q. Zhang, Y. Zhao, S. Yan, Y. Yang, H. Zhao, M. Li, S. Lu, D.L. Kaplan, Preparation of uniaxial multichannel silk fibroin scaffolds for guiding primary neurons, *Acta Biomater.* 8 (2012) 2628–2638.
- [29] A.L. Oliveira, L. Sun, H.J. Kim, X. Hu, W. Rice, J. Kluge, R.L. Reis, D.L. Kaplan, Aligned silk-based 3-D architectures for contact guidance in tissue engineering, *Acta Biomater.* 8 (2012) 1530–1542.
- [30] B. Yetiskin, O. Okay, High-strength silk fibroin scaffolds with anisotropic mechanical properties, *Polymer* 112 (2017) 61–70.
- [31] O. Okay, V.I. Lozinsky, Synthesis and structure–property relationships of cryogels, *Adv. Polym. Sci.* 263 (2014) 103–157.
- [32] V.I. Lozinsky, O. Okay, Basic principles of cryotropic gelation, *Adv. Polym. Sci.* 263 (2014) 49–101.
- [33] I. Karakutuk, F. Ak, O. Okay, Diepoxide-triggered conformational transition of silk fibroin: formation of hydrogels, *Biomacromolecules* 13 (2012) 1122–1128.
- [34] F. Ak, Z. Oztoprak, I. Karakutuk, O. Okay, Macroporous silk fibroin cryogels, *Biomacromolecules* 14 (2013) 719–727.
- [35] B. Yetiskin, C. Akinci, O. Okay, Cryogelation within cryogels: silk fibroin scaffolds with single-, double- and triple-network structures, *Polymer* 128 (2017) 45–56.
- [36] U.J. Kim, J. Park, C. Li, H.J. Jin, R. Valluzzi, D.L. Kaplan, Structure and properties of silk hydrogels, *Biomacromolecules* 5 (2004) 786–792.
- [37] X. Chen, D.P. Knight, Z. Shao, F. Vollrath, Conformation transition in silk protein films monitored by time-resolved Fourier transform infrared spectroscopy: effect of potassium ions on Nephila spidroin films, *Biochemistry* 41 (2002) 14944–14950.
- [38] C. Mo, C. Holland, D. Porter, Z. Shao, F. Vollrath, Concentration state dependence of the rheological and structural properties of reconstituted silk, *Biomacromolecules* 10 (2009) 2724–2728.
- [39] O. Okay, Macroporous copolymer networks, *Prog. Polym. Sci.* 25 (2000) 711–779.
- [40] A. Nisal, R. Sayyad, P. Dhavale, B. Khude, R. Deshpande, V. Mapare, S. Shukla, P. Venugopalan, Silk fibroin micro-particle scaffolds with superior compression modulus and slow bioresorption for effective bone regeneration, *Sci. Rep.* 8 (2018) 7235.
- [41] B. Li, R.M. Aspden, Composition and mechanical properties of cancellous bone from the femoral head of patients with osteoporosis or osteoarthritis, *J. Bone Miner. Res.* 12 (1997) 641–651.
- [42] X. Kong, Y. Qiao, Improvement of recoverability of a nanoporous energy absorption system by using chemical admixture, *Appl. Phys. Lett.* 86 (2005), 151919.
- [43] B.N.J. Persson, *Sliding Friction: Physical Principles and Applications*, 2nd ed. Springer, Heidelberg, 2000.
- [44] J.P. Gong, T. Kurokawa, T. Narita, G. Kagata, Y. Osada, G. Nishimura, M. Kinjo, Synthesis of hydrogels with extremely low surface friction, *J. Am. Chem. Soc.* 123 (2001) 5582–5583.